Appendix A

Verification Tests

A.1 Classic DEM Tests

The example described here is the classic nine-disk test performed in [24], which serves as a verification of the explicit time integration algorithm for the 2D case described in Section 2.1. A simple NURBS intersection-based contact approach is utilized so that the particle overlap is identical with that calculated using equation (2.5). An assembly of nine (9) disks is packed in simple cubic configuration within rigid walls, as shown in Figure A.1. All nine disks are identical, with radius of 50 units and density of 1000 units. Two different contact stiffnesses are used in these calculations: $k_n = 1.35e9$ and $k_n = 1.5e8$, with the shear contact stiffness taken as $k_s = k_n$, unless otherwise noted. Also, the interparticle friction coefficient $\mu = \tan\phi$, where ϕ is the internal friction angle. In this test, $\phi = 15°$, unless otherwise noted. The nine-disk test is subdivided into two loading scenarios: uniform compression and pure distortion.

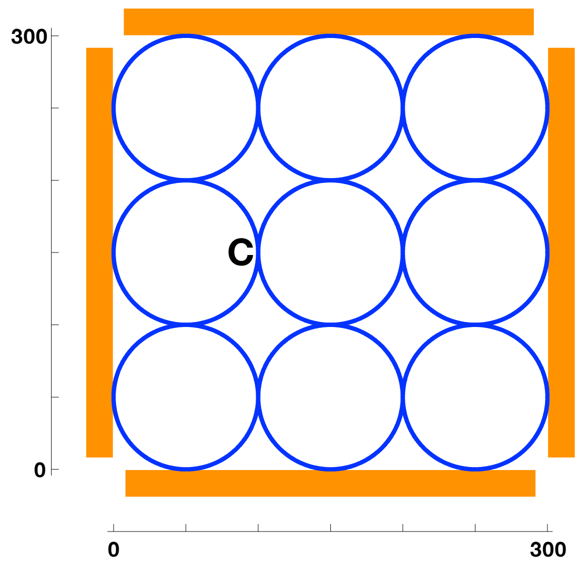

Figure A.1: Initial configuration for nine-disk test.

A.1.1 Uniform compression test

In this test, all four walls are moved inwards with speed v_{wall} for a total duration T_{wall}. Wall motion is then stopped at that point T_{wall} and the test is allowed to continue until a total of 200 cycles is reached. The loading sequences in this test are summarized in Table A.1.

Table A.1: Loading cases for uniform compression test

Case	No.	Disk Stiffness $k_n = k_s$	Δt	T_{wall} (cycles)	v_{wall}
(a)	1	1.35e9	0.01525	40	0.12
	2			120	0.04
(b)	1	1.5e8	0.04576	40	0.36
	2			120	0.12

In this test, the effect of global numerical damping ξ, as it appears on the global equations of motion (see Section 2.1.3), is investigated. Figure A.2 shows the evolution of normal force at point C for case (a) number 1 (see Table A.1). Normal force evolution is reported for the case when there is global numerical damping ($\xi = 3$) and for the case when there is no global damping ($\xi = 0$). No contact damping β is used on any of the results reported herein. The results shown in Figure A.2 exactly match those reported in [24] and clearly show the effect of damping in reducing the amplitude of oscillations, allowing kinematics and corresponding forces to reach steady-state equilibrium. Finally, the evolution of the normal force F_n at point C is shown in Figure A.3. It can be seen from this figure that all loading cases converge to roughly the same value of force after a number of cycles when steady equilibrium is achieved.

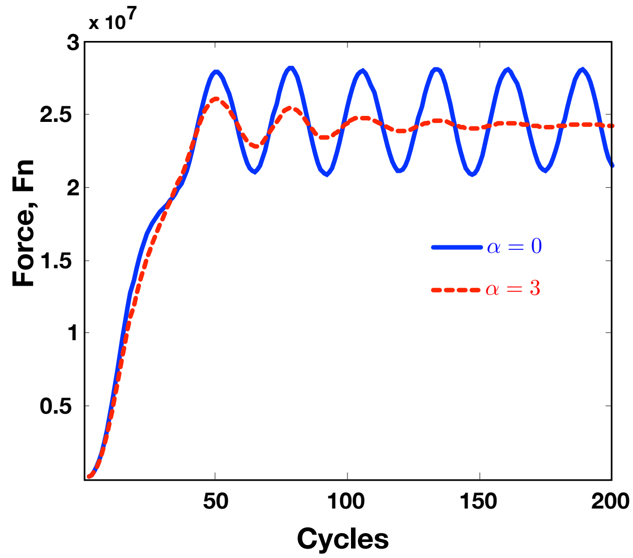

Figure A.2: Normal force F_n evolution at C for loading case (a) No. 1 at different values of global numerical damping.

A.1.2 Distortion test

Here, we reproduce the distortion test for the nine-disk configuration reported in [24]. This constitutes the second half of the verification process and it is performed following the loading sequence reported in [134], which thoroughly describes the distortion test shown in the original work of Cundall and Strack [24]. Similar characteristics, as in Case (a) No. 1 shown in Table A.1, are used here, with $k_n = 1.35e9$ and $\Delta t = 0.01525$. The sample is initially uniformly compressed, as in the uniform compression test, for 4000 cycles with wall speed $v_{wall} = 0.12$, as before. Wall motion is then stopped, followed by 1000 cycles were oscillations are allowed to settle via global numerical damping $\xi = 3.0$. As before, no contact damping was used (i.e., $\beta = 0$). After this uniform and settlement stage (total of 5000 cycles), constant volume distortion is prescribed by rotating the side walls at a constant angular velocity of 0.0175 for 500 cycles. The deformed configuration of the assembly after the first 5000 cycles of uniform compression and settlement, and the subsequent 500 cycles of constant-volume distortion are shown in Figure A.4.

The evolution of the normal force F_n and shear force F_s is shown in Figure A.5. Curves

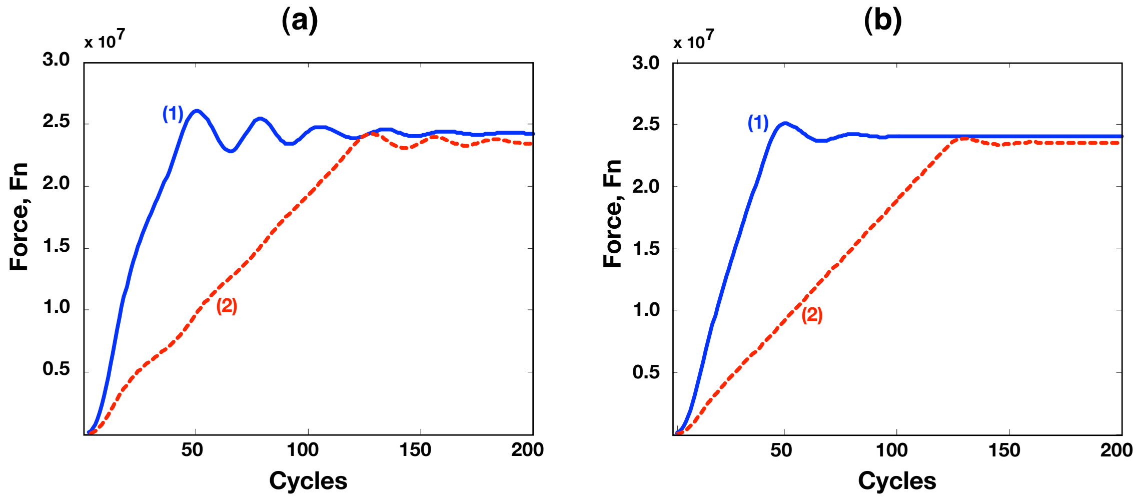

Figure A.3: Evolution of normal force F_n for all loading cases reported in Table A.1 with global numerical damping $\xi = 3$.

are shown for different values of interparticle friction coefficient $\mu = \tan\phi$ at various ratios of normal to shear contact stiffness k_s/k_n. The ratio k_s/k_n was shown by Mindlin [113] to vary from 2/3 to 1 for the case of linear elastic bodies in contact with elliptical contact areas. The extreme values of this range were investigated in [24] and are also reported here in Figure A.5. The evolutions shown in Figure A.5 agree quantitatively with the results obtained in [24; 134] and show the importance of interparticle friction (particle roughness) and the role of contact stiffness as modeled by the ratio k_s/k_n.

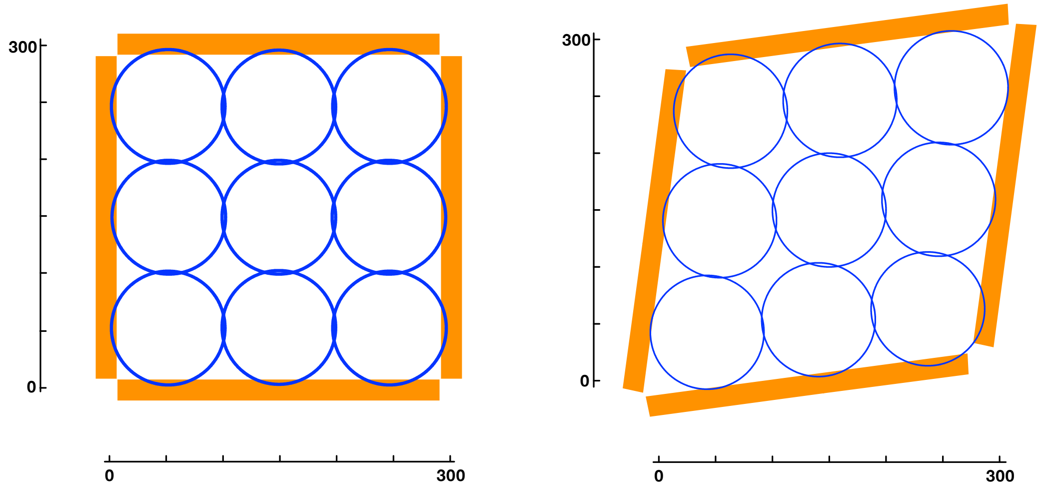

Figure A.4: Distorted configurations for nine-disk assembly after 5000 cycles of uniform compression and settlement, and after a subsequent 500 cycles of constant volume (shear) distortion. Results shown correspond to case when $k_n = k_s$ and interparticle friction angle $\phi = 30°$.

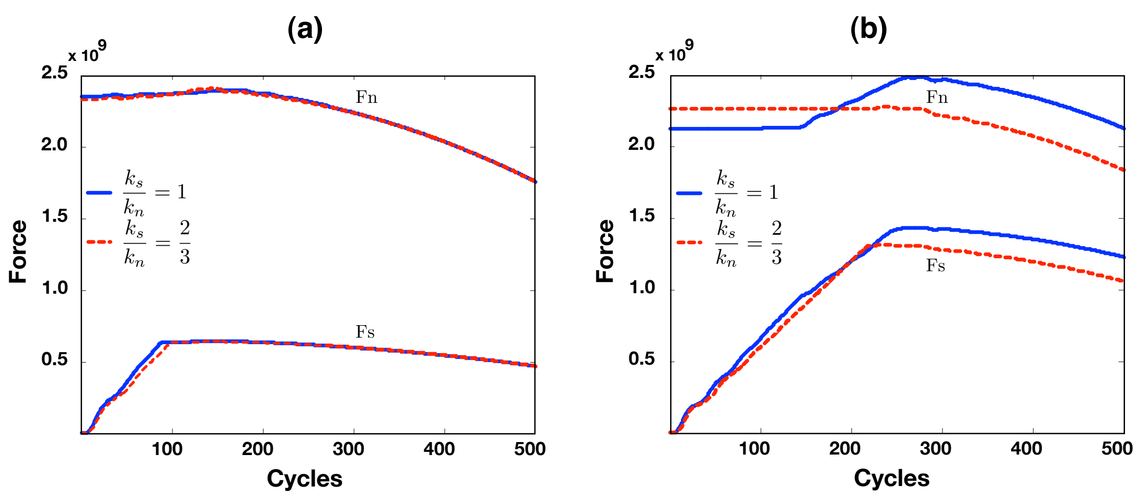

Figure A.5: Normal and shear force evolution at point C in nine-disk assembly during 500 cycle shear distortion at various k_s/k_n ratios. (a) Interparticle friction angle $\phi = 15°$. (b) Interparticle friction angle $\phi = 30°$.

A.2 Contact Dynamics Binary Collision Tests

We check the conservation of energy and momentum under elastic and plastic binary collisions. The left disk (Disk 1) is given an initial velocity of $v_x = 1$ moving towards the right disk (Disk 2), which is stationary. The properties for this problem are mass $m = \pi$, time step $\Delta t = 0.01$, and time stepping parameter $\theta = 0.5$ for elastic collision and $\theta = 1$ for plastic collision.

For elastic collision, the results are shown in Figures A.6 through A.9. We see that both energy and momentum are conserved. After collision, Disk 1 becomes stationary and Disk 2 takes on the velocity $v_x = 1$. For plastic collision, the results are shown in Figures A.10 through A.13. In this case, momentum is conserved, but energy is not. After collision, the Disk 1 and Disk 2 move together at $v_x = 0.5$. These results show that both momentum and energy behave correctly under binary collision.

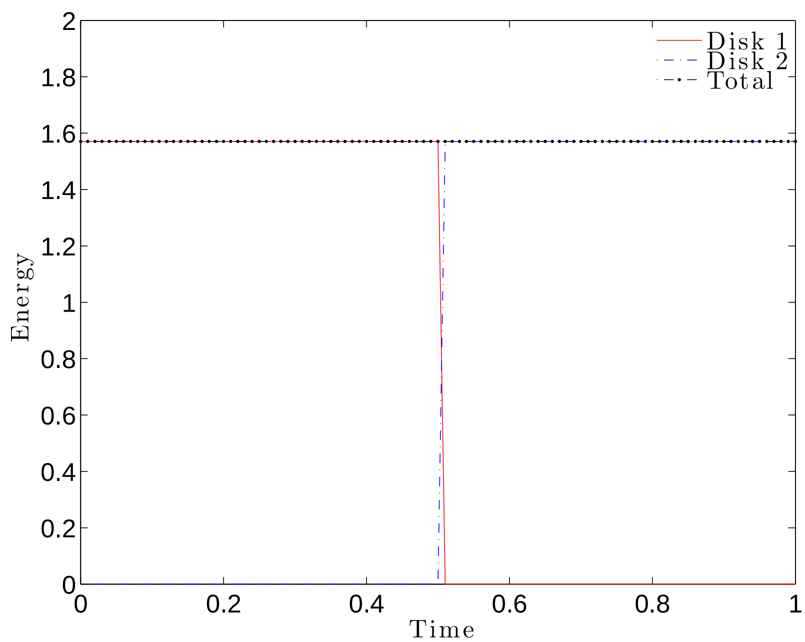

Figure A.6: Elastic collision: energy history.

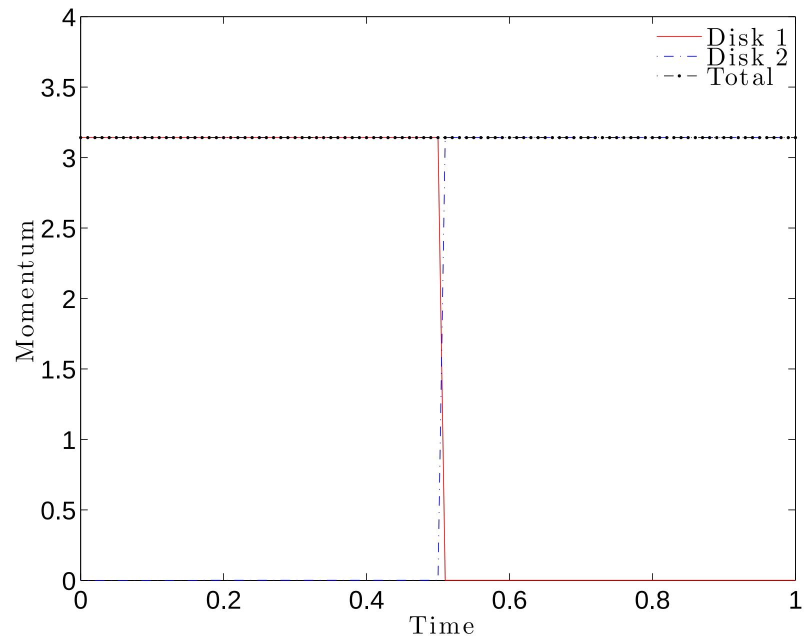

Figure A.7: Elastic collision: momentum history.

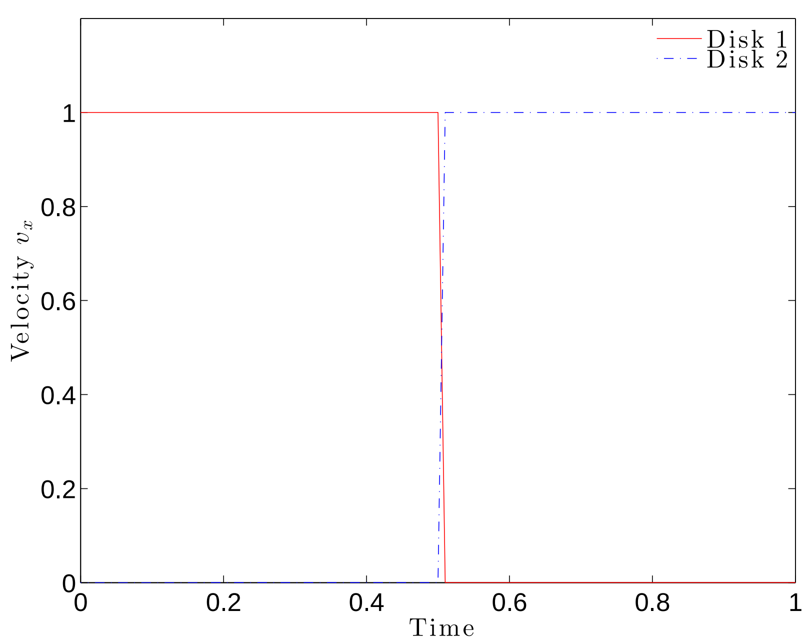

Figure A.8: Elastic collision: velocity v_x history.

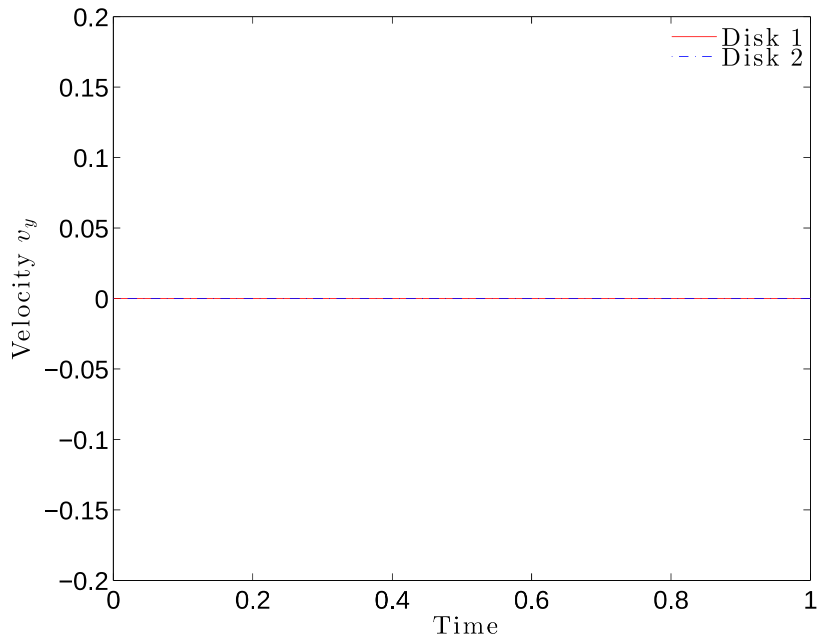

Figure A.9: Elastic collision: velocity v_y history.

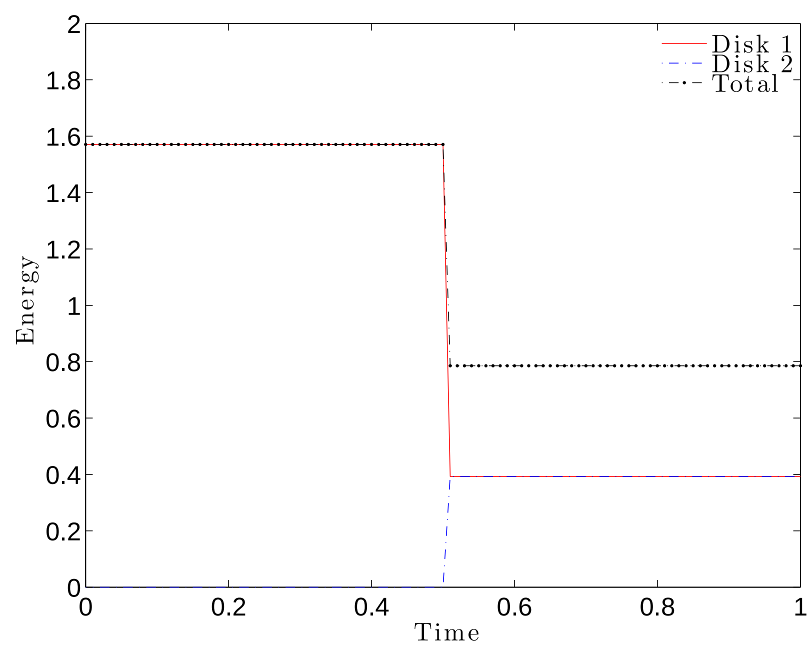

Figure A.10: Plastic collision: energy history.

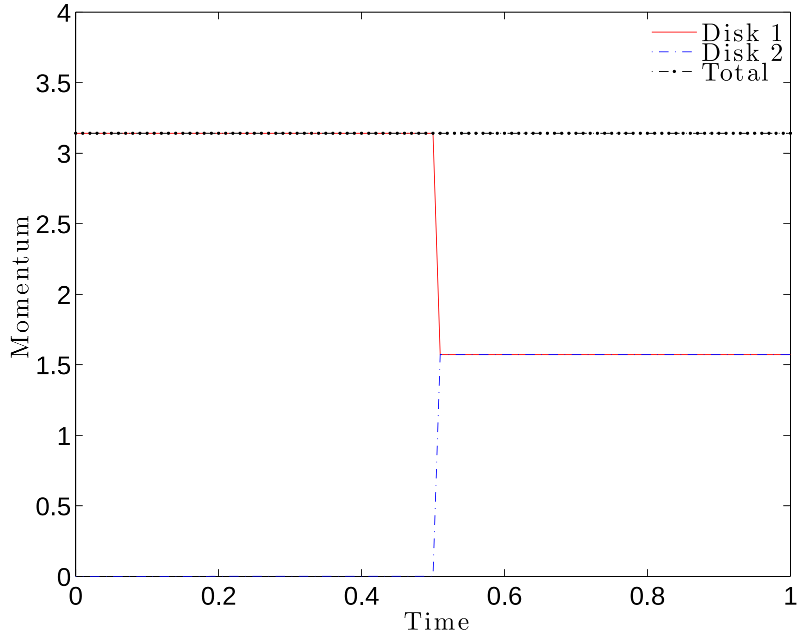

Figure A.11: Plastic collision: momentum history.

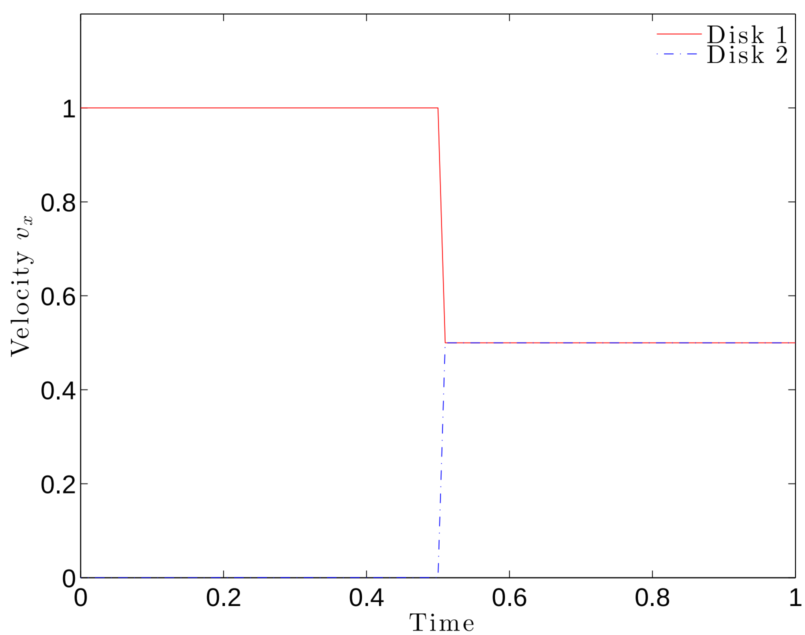

Figure A.12: Plastic collision: velocity v_x history.

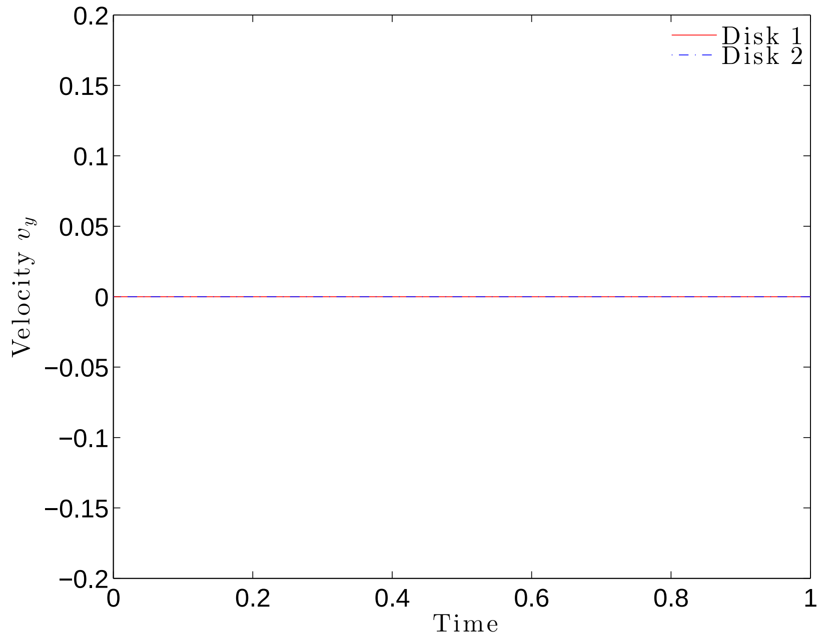

Figure A.13: Plastic collision: velocity v_y history.

A.3 Kinematics with Associated Sliding Rule

In Chapter 4, we presented a CD formulation with an associated sliding rule that introduces a 'dilation layer' between two sliding bodies. Here, we discuss the applicability of this sliding rule. We first discuss the resulting kinematics followed by numerical tests to show that the effects of this rule are very minor, and the slight error made is deemed to be a small price to pay for maintaining a standard convex variational problem. In following the discussion below, the reader should bear in mind the applications in which the associated sliding rule is used, i.e., dense granular media composed of many particles that are being constantly rearranged either with confinement under quasistatic conditons or under dynamic flow conditions. We note that a similar sliding rule, which also introduces a dilation effect, was used by Tasora and Anitescu in their CD formulation [135–139].

A.3.1 Quasistatic case

The presentation here is based on [99]. For clarity, we have excluded rotations and contact elasticity. With this, equation (4.8) reduces to:

$$\begin{aligned}
\min_{\Delta\boldsymbol{x},\Delta\boldsymbol{\alpha}} \; \max_{\boldsymbol{p},\,\boldsymbol{q}} \quad & \left\{\tfrac{1}{2}\Delta\boldsymbol{x}^T\bar{\boldsymbol{M}}\Delta\boldsymbol{x} - \Delta\boldsymbol{x}^T\bar{\boldsymbol{f}}_0\right\} \\
& + \left\{\Delta\boldsymbol{x}^T(\boldsymbol{N}_0\,\boldsymbol{p} + \widehat{\boldsymbol{N}}_0\,\boldsymbol{q}) - \boldsymbol{g}_0^T\boldsymbol{p}\right\} \\
\text{subject to} \quad & \|\boldsymbol{q}\| - \mu\boldsymbol{p} \leq \boldsymbol{0}, \quad \boldsymbol{p} \geq \boldsymbol{0}
\end{aligned} \tag{A.1}$$

The kinematics associated with equation (A.1) are recovered by solving the max part of the problem which leads to the following set of optimality conditions:

$$\begin{aligned}
\Delta\boldsymbol{u}_N &= \boldsymbol{N}_0^T\Delta\boldsymbol{x} = -\mu\boldsymbol{\lambda} + \boldsymbol{g}_0 \\
\Delta\boldsymbol{u}_T &= \widehat{\boldsymbol{N}}_0\Delta\boldsymbol{x} = \operatorname{sgn}(\boldsymbol{q})\boldsymbol{\lambda}
\end{aligned} \tag{A.2}$$

where subscripts N and T denote the normal and tangential directions, respectively, and $\boldsymbol{\lambda}$ are Lagrange multipliers such that $\lambda^I(|q^I| - \mu p^I) = 0, I \in C$, where C is the set of potential contacts. The important point regarding the above kinematic equations is that the gap g_0 in time discrete processes tends to cancel the dilation and in such a way that is entirely eliminated in the limit of the time step tending to zero. This can be illustrated by the simple example shown in Figure A.14. We here consider a single particle on a rigid

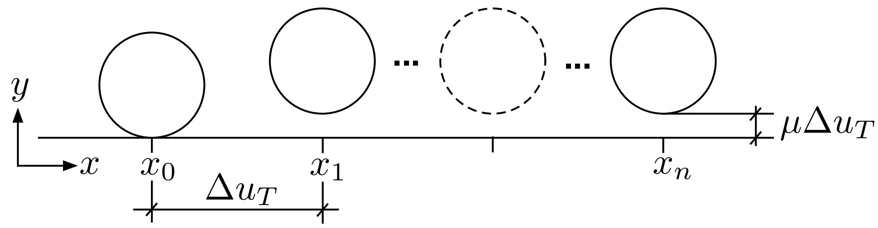

Figure A.14: Quasistatic sliding along a rigid frictional surface.

frictional surface. The particle is initially at rest on the surface at $(x_0, y_0) = (x_0, 0)$ As such, the gap between the particle and the surface is $g_0 = 0$. A series of tangential displacements $\Delta u_T = \Delta u_x$ of equal size are then imposed in a quasistatic manner. With the application of the first increment, the normal displacement is $-\Delta u_{N,1} = \Delta u_{y,1} = \mu\Delta u_{x,T}$ which brings the particle to position $(x_1, y_1) = (x_0 + \Delta u_T, \mu\Delta u_T)$. To continue the time stepping, the new gap is calculated as $g_1 = \mu\Delta u_T$. From equation (A.2), the new normal displacement then follows as $\Delta u_{N,2} = g_1 - \mu\Delta u_T = 0$. In other words, no further dilation occurs and the particle slides parallel to the surface at a distance $\mu\Delta u_T$ above it such that an artificial dilation layer — which can be made arbitrarily thin — separates the particle from the surface. Despite this physical separation, contact forces still exist and the behavior of the particle is in every way equal to what it would be with a gap identically equal to zero.

A.3.2 Dynamic case

To study the more general dynamic case, we consider a particle as shown in Figure A.15. The particle is initially at a distance g_0 from the rigid frictional surface located at $y = 0$

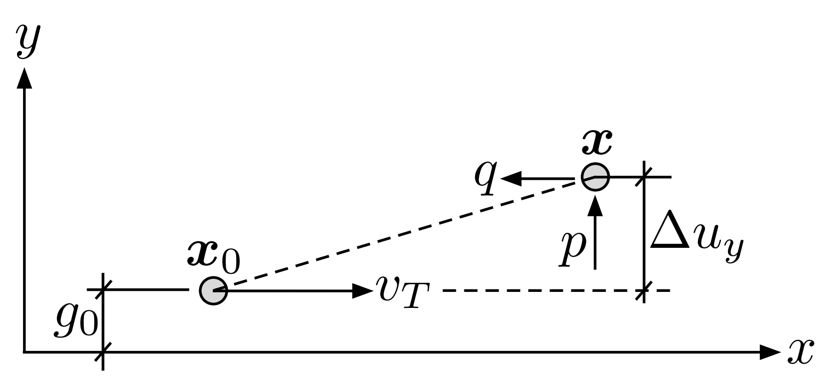

Figure A.15: Dynamic sliding along a rigid frictional surface.

and has an initial horizontal velocity v_T. It is assumed that the particle is within the zone of contact, i.e., within the dilation layer introduced above. This will possibly bring about a further dilation such that the gap increases or the particle may slide along the initial dilation layer as in the quasistatic case. The time discrete governing equations (for $\theta = 1$) are given by (see Section 4.2.3)

$$\begin{aligned} m\Delta u_x &= -q\Delta t^2 + m v_T \Delta t \\ m\Delta u_y &= p\Delta t^2 \\ q &= \mu p \\ \Delta u_x &= \lambda \\ \Delta u_y &= \mu\lambda - g_0 \end{aligned} \tag{A.3}$$

From these equations, the vertical displacement is found to be

$$\Delta u_y = \frac{\mu v_T \Delta t - g_0}{1 + \mu^2} \tag{A.4}$$

Equating the numerator to zero leads us to define a critical time step:

$$\Delta t_{\mathrm{cr}} = \frac{g_0}{\mu v_T} \tag{A.5}$$

such that the initial gap will not grow any further for $\Delta t \leq \Delta t_{\mathrm{cr}}$ while it will increase for $\Delta t > \Delta t_{\mathrm{cr}}$. In other words, for a finite initial gap, a time step can always be chosen to produce a non-dilative response. This property breaks down for an initial gap identically equal to zero. In this case, the response will be dilative, regardless of the time step. In practice, however, the effects of this possible dilation are in most cases very limited as will be shown in Section A.3.4.

A.3.3 The case with rotations included

From equation (4.14), the kinematic relations with rotations included (but without contact elasticity) are:

$$\begin{aligned} \Delta \boldsymbol{u}_N &= \boldsymbol{N}_0^T \Delta \boldsymbol{x} = \boldsymbol{g}_0 - \mu\boldsymbol{\lambda} \\ \Delta \boldsymbol{u}_T &= \widehat{\boldsymbol{N}}_0^T \Delta \boldsymbol{x} = \mathrm{sgn}(\boldsymbol{q})\boldsymbol{\lambda} + (\boldsymbol{R}_0^{qT} + \boldsymbol{R}_0^{pT})\Delta\boldsymbol{\alpha} \end{aligned} \tag{A.6}$$

In this case, the inclusion of rotations further limits dilation in the sense that tangential motion can be accommodated not only by sliding ($\boldsymbol{\lambda} > \mathbf{0}$), but also by rolling ($|\Delta\boldsymbol{\alpha}| > \mathbf{0}$). This lends further credence to the approach of using an associated sliding rule. Indeed, in the quasistatic deformation of granular materials, such as in triaxial tests, it has long been recognized that sliding occurs only at a small fraction of the contacts [82].

A.3.4 A numerical test

To see the consequence of the associated sliding rule, and show that its effects are very minor for the types of granular media applications mentioned above, consider the problem of a block on an incline as shown in Figure A.16. We solve this problem using the CD formulation described in Chapter 4, without contact elasticity in which the effects of the associated sliding rule are most prominent. The properties for this problem are incline angle $\theta_\mathrm{s} = 20°$, block mass $m = 7.854$, and acceleration of gravity $g = 10$. The critical friction coefficient is $\mu_\mathrm{crit} = \tan\theta_\mathrm{s} = 0.364$. The friction coefficient between the block and incline is

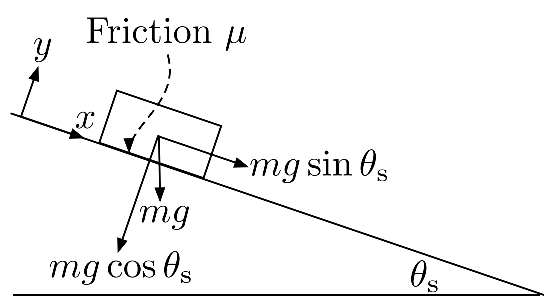

Figure A.16: Block on an incline.

denoted by μ. We consider two cases:

1. $\mu = 0.36 < \mu_\mathrm{crit}$, which means that the block should slide down
2. $\mu = 0.4 > \mu_\mathrm{crit}$, which means that the block should remain stationary

For the block starting from rest, the exact solution is:

$$
\begin{aligned}
x(t) &= \begin{cases} 0 & : \mu > \mu_{\text{crit}} \\ 0.5(\sin\theta_s - \mu\cos\theta_s)gt^2 & : \mu < \mu_{\text{crit}} \end{cases} \\
\dot{x}(t) &= \begin{cases} 0 & : \mu > \mu_{\text{crit}} \\ (\sin\theta_s - \mu\cos\theta_s)gt & : \mu < \mu_{\text{crit}} \end{cases}
\end{aligned}
\tag{A.7}
$$

The time stepping parameter is set at $\theta = 1$ and we consider three time steps $\Delta t = 0.01, 0.005$ and 0.0025. We observe that for Case 1 (see Figures A.17 through A.21), the sliding block is accompanied by a negligible dilation that grows at a very small rate as shown in Figure A.19, and this dilation decreases as the time step gets smaller. These observations are consistent with the kinematic analysis for the dynamic case with zero initial gap described in the previous section. The dilatation did not affect the calculated contact normal and shear forces, which match mg and μmg, respectively. Again, we emphasize that in the aforementioned granular applications, a sliding particle would typically move for a very short distance before kinematically affected by its neighboring particles in the next time step, and the associated dilation within a time step would be a negligible fraction of the particle size. For Case 2 (see Figures A.22 through A.26), the block remained stationary as expected.

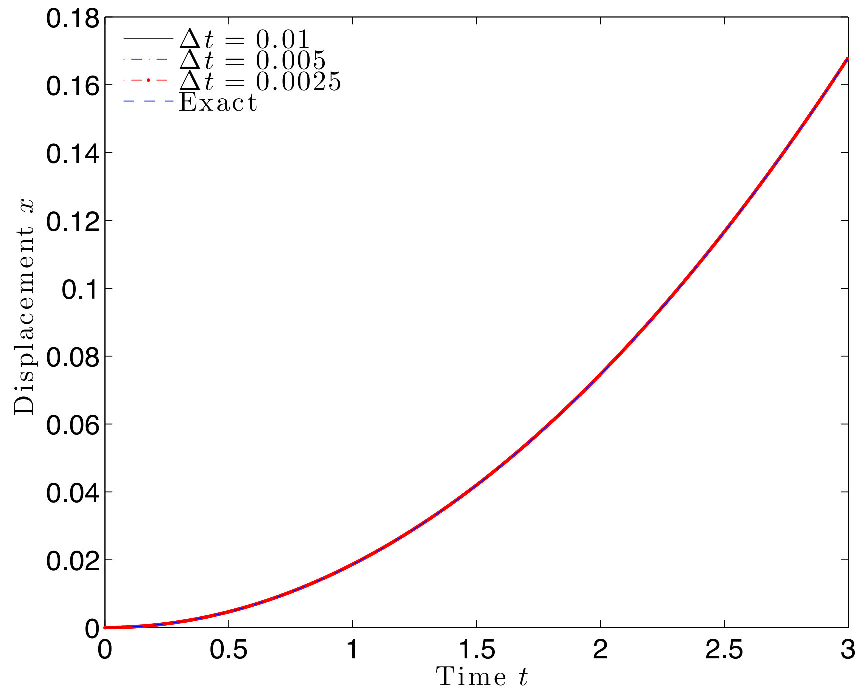

Figure A.17: Displacement along x ($\mu = 0.36$).

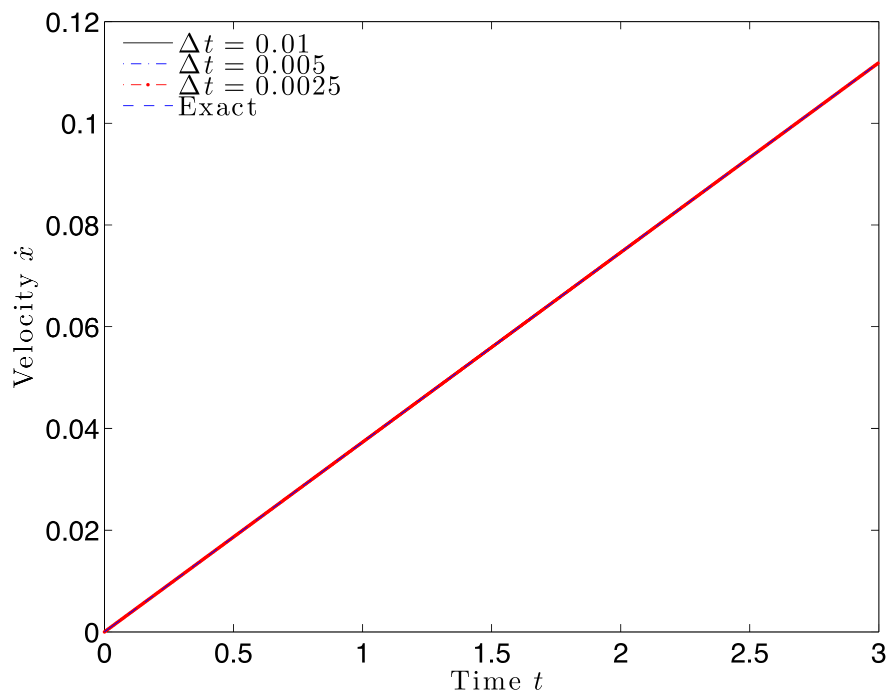

Figure A.18: Velocity along x ($\mu = 0.36$).

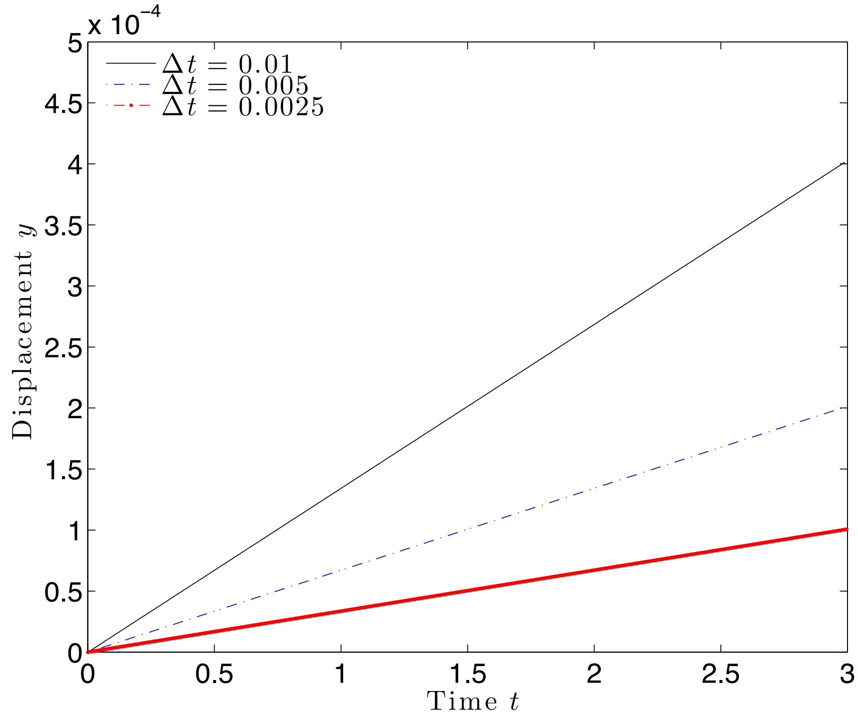

Figure A.19: Displacement normal to plane or gap ($\mu = 0.36$).

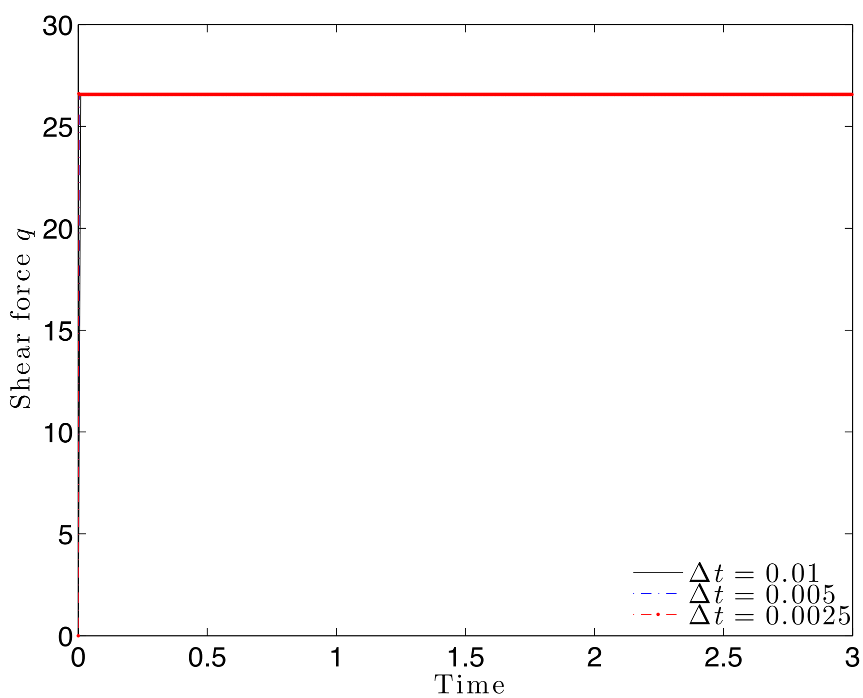

Figure A.20: Shear force ($\mu = 0.36$).

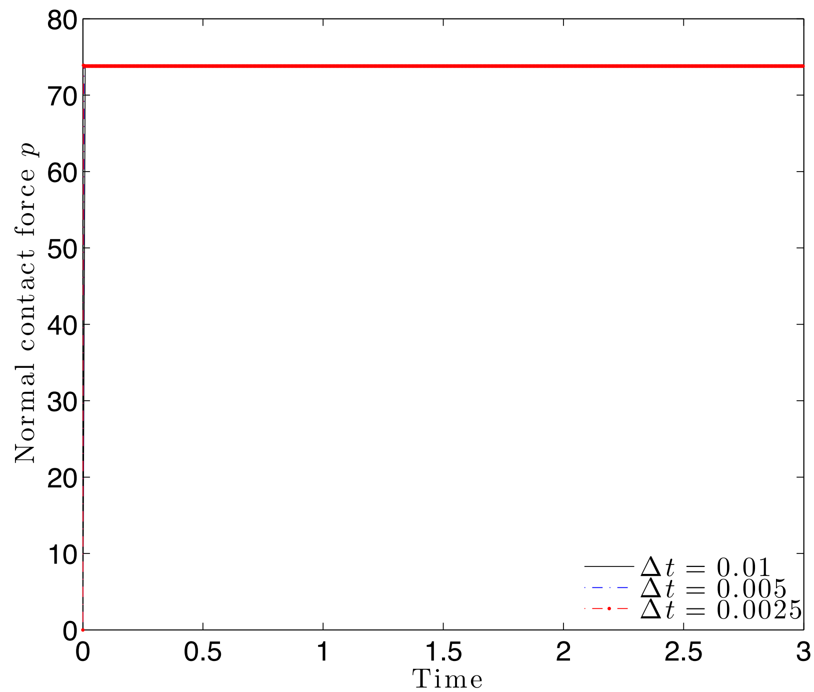

Figure A.21: Normal contact force ($\mu = 0.36$).

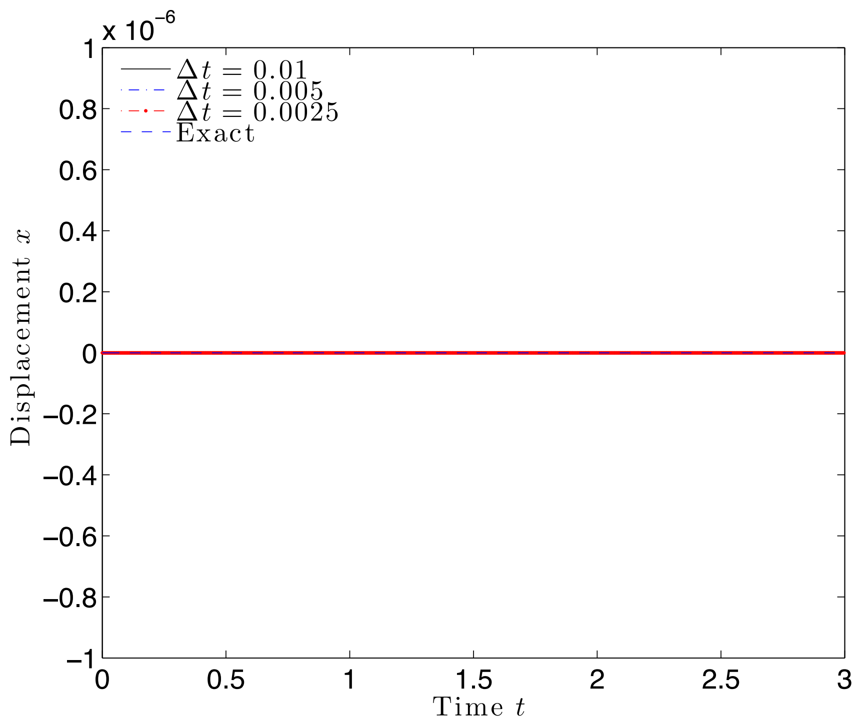

Figure A.22: Displacement along x ($\mu = 0.4$).

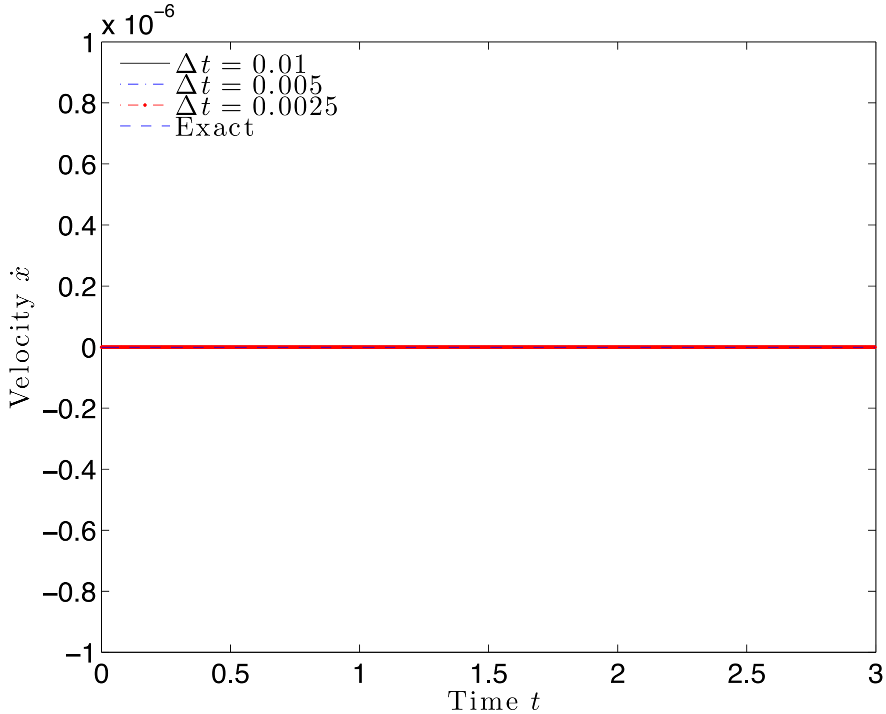

Figure A.23: Velocity along x ($\mu = 0.4$).

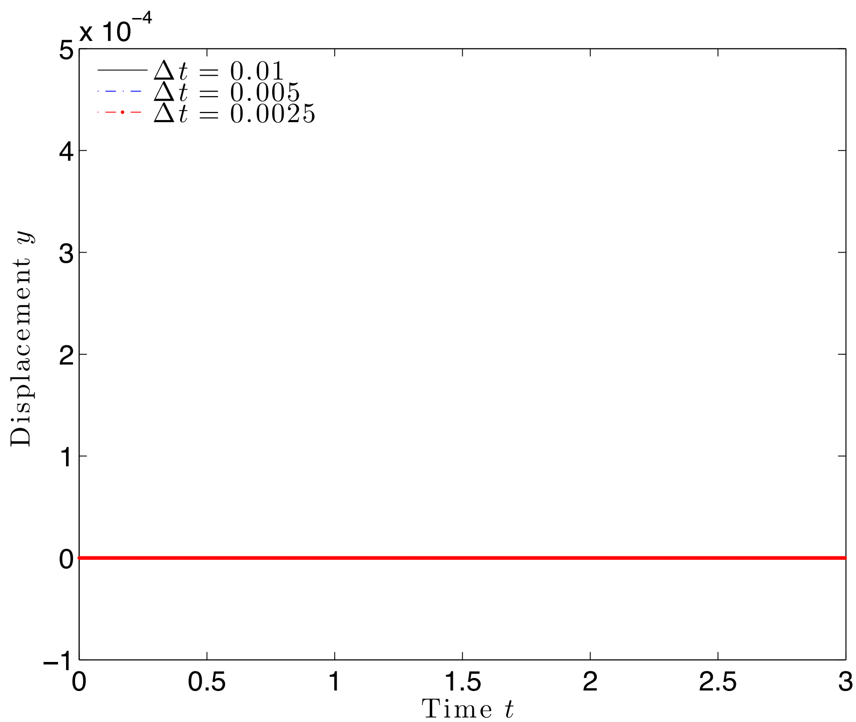

Figure A.24: Displacement normal to plane or gap ($\mu = 0.4$).

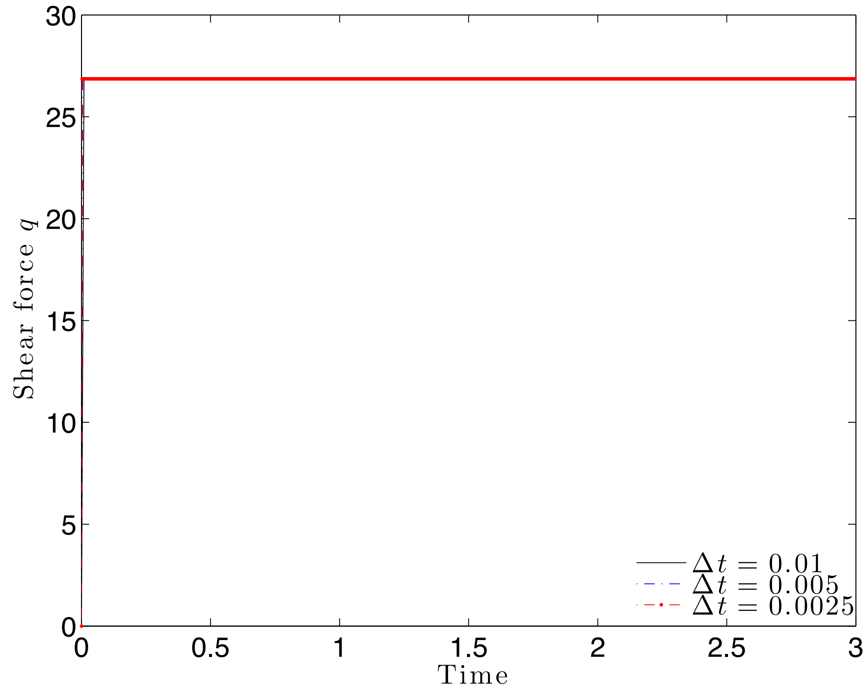

Figure A.25: Shear force ($\mu = 0.4$).

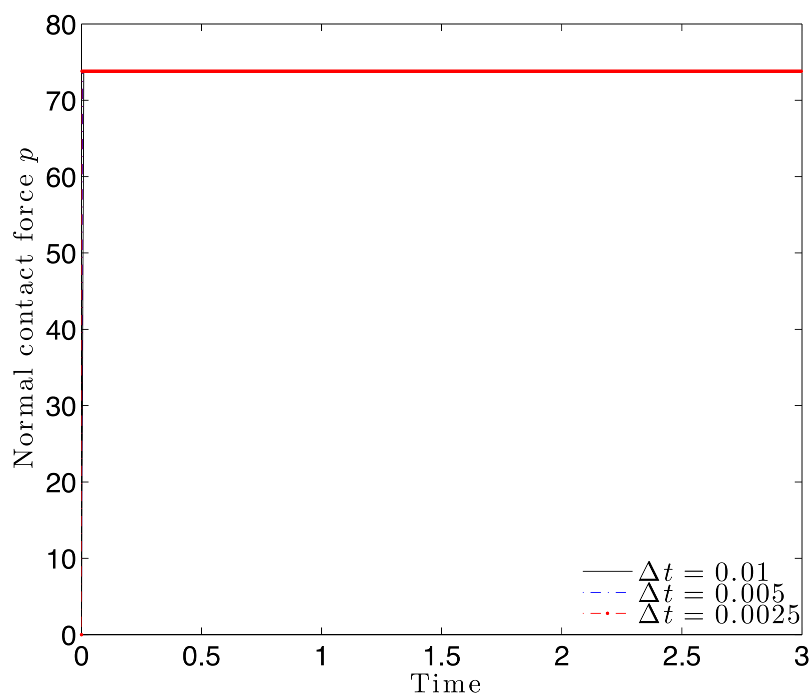

Figure A.26: Normal contact force ($\mu = 0.4$).